

CrossMark  
click for updates

Cite this: DOI: 10.1039/c5tc00276a

## Highly conductive PEDOT:PSS films by post-treatment with dimethyl sulfoxide for ITO-free liquid crystal display

Tsu-Ruey Chou,<sup>a</sup> Szu-Hua Chen,<sup>a</sup> Yen-Te Chiang,<sup>b</sup> Yi-Ting Lin<sup>a</sup> and Chih-Yu Chao<sup>\*abc</sup>

In this study, a simple and effective method to enhance the conductivity of poly(3,4-ethylenedioxythiophene):poly(styrenesulfonate) (PEDOT:PSS) thin films from 0.7 to 1185 S cm<sup>-1</sup> by post-treatment with dimethyl sulfoxide (DMSO) is demonstrated. After the rubbing technique was applied, the DMSO-treated PEDOT:PSS film could be used as both the transparent electrode and the alignment layer to fabricate ITO-free liquid crystal (LC) cells. The electro-optical properties of LC cells fabricated by the rubbed PEDOT:PSS were comparable to those constructed by ITO and polyimide. This work indicates that the highly conductive PEDOT:PSS film is a promising material for ITO-free LC devices.

Received 28th January 2015,  
Accepted 25th February 2015

DOI: 10.1039/c5tc00276a

www.rsc.org/MaterialsC

### Introduction

Optoelectronic devices such as liquid crystal displays (LCDs), organic photovoltaics (OPVs) and organic light-emitting diodes (OLEDs) have received great interest these years due to their mechanical flexibility, light weight, and prospective potential for roll-to-roll manufacturing. Among these devices, LCD has been commercialized since at least 30 years and has become the most widely used display in our daily life. Recently, researchers have developed several new modes of liquid crystal (LC) devices to achieve high performance display, *e.g.*, in-plane switching,<sup>1</sup> patterned vertical alignment,<sup>2</sup> and fringe-field switching.<sup>3</sup> No matter in which modes, LC devices act as a light valve to control the transmission of backlight. Therefore, the transparent electrode is required for LC device architecture, even in the case of reflective LCDs.

Indium tin oxide (ITO), which could be deposited on both glass and plastic substrates, has been the most commonly used material as the transparent electrode for decades. However, the limited indium on earth and the fragile characteristic of ITO thin films increase the cost of LCDs and restrict the applicability of ITO on flexible electronic devices, respectively.<sup>4–6</sup> Furthermore, the total reflection at the glass/ITO interface,<sup>7</sup> poor transparency in the blue spectrum,<sup>8</sup> and poor adhesion to

organic materials degrade the performance of optoelectronic devices which use ITO as the transparent electrode. These drawbacks make ITO a non-ideal material in the future, and thus searching for an alternative to replace ITO is an unavoidable task.

To date, many materials such as carbon nanotube,<sup>9–12</sup> metal nanowires,<sup>13,14</sup> thin metal,<sup>15</sup> graphene,<sup>16,17</sup> and conducting polymers<sup>18–20</sup> have been investigated as alternatives to replace ITO. In particular, poly(3,4-ethylenedioxythiophene):poly(styrenesulfonate) (PEDOT:PSS) is one of the most potential materials due to its excellent mechanical flexibility, good thermal stability, and high transparency in the visible range. It can be dispersed in water and several organic solvents and hence PEDOT:PSS films could be prepared by simple solution processes such as spin coating or inject printing.<sup>21–23</sup> However, the conductivity of the pristine PEDOT:PSS film, typically below 1 S cm<sup>-1</sup>, is extremely lower than that of the commercialized ITO, which makes it inappropriate for practical applications. The insulating PSS, which makes the conductive PEDOT to be easily dispersed in water, is the main reason for the low conductivity of PEDOT:PSS films. In order to improve the conductivity of PEDOT:PSS, several methods have been reported, including doping additional organic compounds with their boiling points higher than the boiling point of water, such as dimethyl sulfoxide (DMSO),<sup>24</sup> ionic liquid,<sup>25</sup> dimethyl sulfate,<sup>26</sup> or polyol,<sup>27</sup> into PEDOT:PSS aqueous solution and processing post-treatment of PEDOT:PSS films with cosolvents,<sup>28</sup> ethylene (EG),<sup>29</sup> salt,<sup>30</sup> or inorganic acid.<sup>31</sup> Generally speaking, doping polar solvents into PEDOT:PSS leads to morphology changes including extended grain size and better interconnection between PEDOT chains, whereas post-treatment usually results in both morphology changes and removal of unwanted PSS on the film surface. Therefore, methods including

<sup>a</sup> Department of Physics, National Taiwan University, No. 1, Sec. 4, Roosevelt Rd., Taipei 10617, Taiwan. E-mail: cychao@phys.ntu.edu.tw

<sup>b</sup> Institute of Applied Physics, National Taiwan University, No. 1, Sec. 4, Roosevelt Rd., Taipei 10617, Taiwan

<sup>c</sup> Molecular Imaging Centre, National Taiwan University, No. 1, Sec. 4, Roosevelt Rd., Taipei 10617, Taiwan

post-treatment usually show better results than those simply using additives to improve the conductivity of PEDOT:PSS films.

In this paper, the conductivity enhancement of highly conductive PEDOT:PSS films through post-treatment with DMSO was performed. The conductivity enhanced greatly by four orders of magnitude, which is attributed to the removal of PSS on the surface and the conformational change of the PEDOT:PSS film. After we implemented the rubbing technique with a polyester cloth, the DMSO-treated highly conductive PEDOT:PSS films revealed uniform planar alignment which could be used as the alignment layer in the LC device. The measured electro-optical properties show comparable characteristics relative to those of LC cells assembled by the polyimide (PI) coated ITO glass. Here our work shows the potential and facility of highly conductive PEDOT:PSS films that can be used as both the transparent electrode and the alignment layer in LC devices for ITO-free LC displays.

## Experimental

The PEDOT:PSS aqueous solution (Clevios PH1000) was purchased from Heraeus Clevios GmbH with a solid concentration 1.0–1.3 wt% and the weight ratio of PEDOT to PSS was 0.4. DMSO (99.9%, anhydrous) was purchased from Sigma-Aldrich with a water content less than 0.005 wt%. All the materials were used without further purification. The chemical structures of these materials are shown in Scheme 1.

Glass substrates ( $2.5 \times 2.5 \text{ cm}^2$ ) were cleaned with detergent, acetone, isopropyl alcohol and deionised (DI) water successively. After drying in the oven, glass substrates were treated with air plasma for 4 min to enhance the wettability. A single-layer PEDOT:PSS thin film was deposited on a glass substrate *via* spin coating at 3000 rpm for 60 s and then annealed at  $120^\circ \text{C}$  for 15 min. The PEDOT:PSS aqueous solution was filtered through a  $0.45 \mu\text{m}$  syringe filter prior to spin coating. Next, a small amount of DMSO was dropped directly (hereafter referred as the ‘drop’

method) on the PEDOT:PSS film at  $120^\circ \text{C}$  and dried for 15 min. The treated film was then rinsed with DI water several times to remove the excess PSS on the film and finally dried at  $120^\circ \text{C}$  for 15 min again. Thicker PEDOT:PSS films were prepared by multiple coatings and treated in the same way described above on each PEDOT:PSS layer.

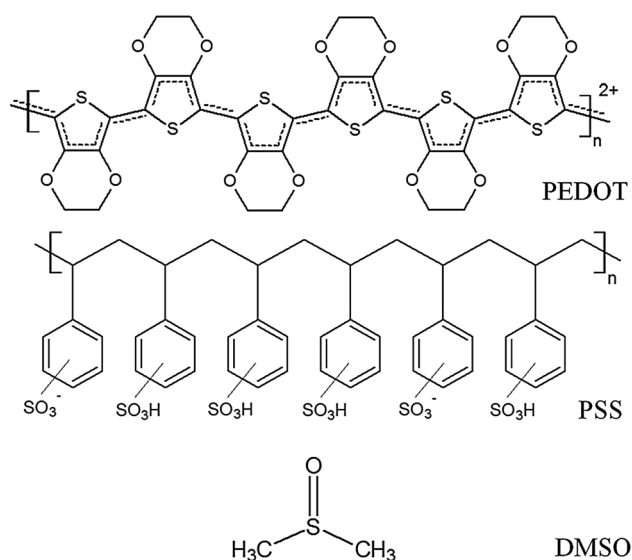
The sheet resistance ( $R_s$ ) of PEDOT:PSS films was measured by the four point probe method and the electrical conductivity ( $\sigma$ ) was calculated using the formula:

$$\sigma = 1/(R_s \times d) \quad (1)$$

where  $d$  is the film thickness. The surface morphology and the thickness of the PEDOT:PSS film were characterized and measured by means of an Park XE-100 atomic force microscope (AFM) operated in tapping mode. The resonance frequency of the tip (PPP-RT-NCHR, Nanosensors) we used in this study was 330 kHz. Raman spectra were measured using a Horiba Jobin Yvon HR800 confocal  $\mu$ -Raman system. The wavelength and power of the excitation laser are 633 nm and 5.4 mW, respectively. Optical transmission and absorption spectra were taken using a UV-vis-NIR spectrometer (JASCO V-670).

The empty LC cells were fabricated using two glass substrates coated with double layers of highly conductive PEDOT:PSS films. The top layer was rubbed with a polyester cloth after post-treatment in order to yield a unidirectional planar alignment. Besides, empty LC cells constructed from ITO glass (sheet resistance  $95 \Omega \square^{-1}$ ) coated with a polyimide layer (AL-12G, Daily-Polymer) were made for comparison. The cell configuration of all samples is  $90^\circ$  twisted nematic (TN) mode with a  $4 \mu\text{m}$  cell gap ensured by silica spacers. Thereafter, nematic LCs (DF-7538A, Daily-Polymer) were injected into empty cells by means of capillary action in the isotropic phase. The structures of LC cells fabricated using glass/PEDOT:PSS and glass/ITO/PI are shown in Fig. 1.

After sample preparation, polarizing optical microscopy (POM) was employed to examine the uniformity of the LC alignment. The voltage–transmittance ( $V$ – $T$ ) curve and response time of each cell from a He–Ne laser source were measured using a silicon photo detector. All cells were placed between a pair of cross-polarizers and measured by applying a square wave voltage with a frequency of 1 kHz in the normally white mode.



Scheme 1 Chemical structures of PEDOT, PSS, and DMSO.

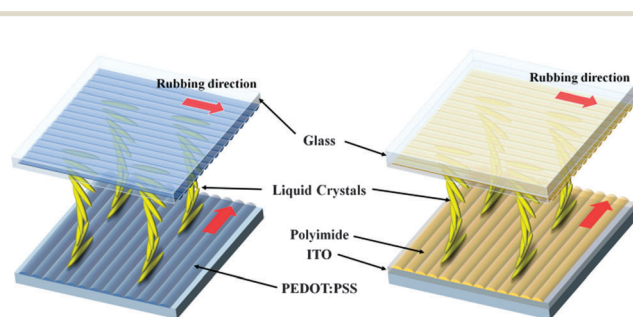


Fig. 1 The structure of LC cells fabricated using the rubbed highly conductive PEDOT:PSS on glass and polyimide on ITO glass.

## Results and discussion

Previous reports have shown that adding a small amount of DMSO or other solvents into high conductive PH 1000 PEDOT:PSS could enhance the conductivity of the PEDOT:PSS film.<sup>24</sup> Besides, some studies showed conductivity enhancement upon immersing the dried PEDOT:PSS film into EG or treatment with polar solvent or cosolvents.<sup>28,29,31</sup> Therefore, we are interested in which method shows the best result using DMSO. Fig. 2 shows the conductivities along with the error bar of the pristine PEDOT:PSS and after three conductivity enhancing methods using anhydrous DMSO. The '5% DMSO' was done by mixing 5% (v/v) DMSO in the PEDOT:PSS aqueous solution and stirred for 24 h prior to spin coating. The 'dip' treatment was performed by immersing the annealed PEDOT:PSS film into DMSO at room temperature for 30 min and dried at 120 °C for 15 min. The drop method was done using the procedure mentioned in the experimental section. The average conductivity increased from 0.7 S cm<sup>-1</sup> to 755, 789, 994 S cm<sup>-1</sup> for samples with 5% DMSO, treated with the dip method, and treated with the drop method, respectively. Obviously, the drop method shows the best result compared with the others. Therefore, the drop method was adopted as the post-treatment process for the following experiments in this study.

Previously, Xia and Ouyang demonstrated that the conductivity of PEDOT:PSS film could be enhanced by post-treatment with cosolvents including water, methanol, ethanol, 1,2-dichlorobenzene, *etc.* They carried out a study to find out whether anhydrous methanol or normal methanol (water less than 0.05%) is a better candidate to enhance the conductivity of the less conductive PEDOT:PSS (Clevios VP AI4083), which is often used as a buffer layer in OLED or OPV cells. Their results showed that the conductivity of the less conductive PEDOT:PSS film treated with normal methanol improved more than those treated with anhydrous methanol.<sup>28</sup> This indicates that even a small amount of water in the normal methanol could influence the result of post-treatment. Motivated by this study, we added a small amount of DI water into the anhydrous DMSO. In our experiments, the concentration of DI water varied from 0 to 6% (v/v). Fig. 3 shows the variation of the conductivity of PEDOT:PSS films treated with DMSO doped with different concentrations of DI water.

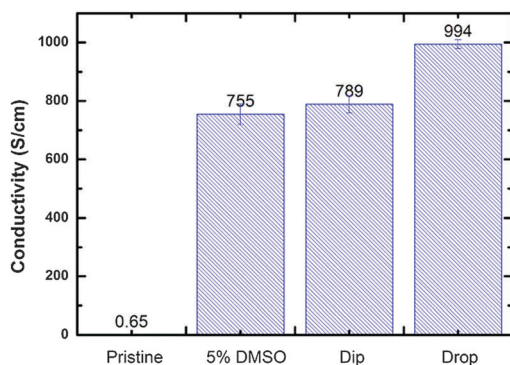


Fig. 2 Conductivities of PEDOT:PSS films treated with DMSO by different methods.

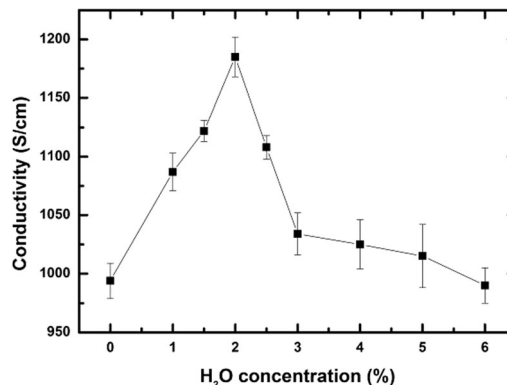


Fig. 3 Variation of the conductivity of PEDOT:PSS films treated with DMSO doped with different concentrations of DI water.

The highest conductivity (1185 S cm<sup>-1</sup>) was obtained when the doping concentration was 2%. The conductivity decreased gradually when the doping concentration was above 3%.

Various mechanisms have been proposed to explain the conductivity enhancement of PEDOT:PSS films. For those methods utilizing the post-treatment process, two mechanisms contribute to the conductivity enhancement mainly: the removal of those excess PSS on the surface of the PEDOT:PSS film and the conformational change of the PEDOT and PSS chain. The surface of the pristine PEDOT:PSS film contains more PSS than the bulk region.<sup>32</sup> Therefore, removing the hygroscopic and insulating PSS on the film surface is crucial to increase the stability and conductivity of PEDOT:PSS. Fig. 4 shows the UV absorption spectra of the pristine and the DMSO-treated PEDOT:PSS films. The two absorption peaks at 195 nm and 225 nm correspond to the aromatic rings of PSS.<sup>33</sup> From Fig. 4, it is clear that the intensity of these two bands decreased after DMSO post-treatment, which implies that the amount of PSS chains in the PEDOT:PSS film reduced after the post-treatment. Besides, after the DMSO post-treatment, the film thickness reduced from 60 nm to 40 nm, which is attributed to the removal of PSS chains.

The PEDOT and PSS form a core-shell structure in the pristine film where the core region is conductive PEDOT rich

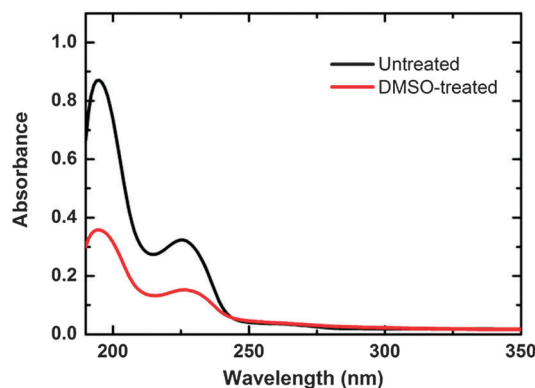


Fig. 4 UV absorption spectra of PEDOT:PSS films before and after the DMSO post-treatment.

and the shell region is insulating PSS rich.<sup>34</sup> Since the conductive core is surrounded by the insulating shell, it is hard for those carriers on the PEDOT chain to transport through the film, and thus the pristine film shows low conductivity. The surface topography and phase images of the PEDOT:PSS film before and after the DMSO post-treatment were captured by AFM, as shown in Fig. 5. From Fig. 5(a) and (b), it is clear that the PEDOT:PSS film turned from a core-shell structure to an entangled wire-like structure after the post-treatment. This conformational change is attributed to the DMSO post-treatment which reduces the Coulombic attraction between PEDOT and PSS. The reduced attraction results in phase separation between the hydrophobic PEDOT and hydrophilic PSS. Along with the removal of PSS, PEDOT chains turned from a coiled to a linear structure, as shown in Fig. 5(c) and (d). This conformational change reduces the energy barrier of charge hopping on the PEDOT:PSS film which contributes to the conductivity enhancement. The surface roughness (mean roughness) increased from 1.14 nm to 1.56 nm after the post-treatment, which is still acceptable smoothness. To further confirm the conformational change of PEDOT:PSS films after the DMSO post-treatment, Raman spectroscopy was performed. Fig. 6 shows the Raman spectra of the pristine and the DMSO-treated PEDOT:PSS films. The strongest band between 1400 and 1500  $\text{cm}^{-1}$  corresponds to the  $C_{\alpha}=C_{\beta}$  symmetric stretching of the five-membered thiophene ring on the PEDOT chains.<sup>35,36</sup> The peak value of this band is red shifted from 1427 to 1414  $\text{cm}^{-1}$  after the post-treatment, which indicates that the resonant structure of the PEDOT chains changes from the benzoid structure to the quinoid structure.<sup>35,37</sup> The benzoid structure

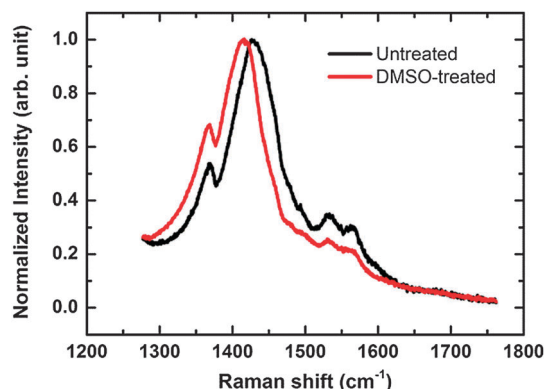


Fig. 6 Raman spectra of PEDOT:PSS films before and after the DMSO post-treatment.

is the favoured structure for the coil conformation while the quinoid structure is the favoured structure for the expanded-coil or the linear conformation.<sup>38</sup> Therefore, the measured red shift in Raman spectra confirms the conformational change of the PEDOT chains after we performed the DMSO post-treatment.

In order to reduce the sheet resistance of the PEDOT:PSS film, multilayer architecture was obtained. This can be obtained by spin coating the PEDOT:PSS solution multiple times. The post-treatment was carried out on each layer with 2% DI water doped DMSO. The sheet resistance reduced from 211 to 103 and 67  $\Omega \square^{-1}$  for single layer, double layers and triple layers, respectively. The conductivity of the third layer is slightly lower, which is similar to the result of other groups.<sup>31</sup> The sheet resistances of the multilayer film are comparable to or lower than that of the ITO substrate used for LC devices, which has a typical value of about 100  $\Omega \square^{-1}$ . On the other hand, Fig. 7 presents the transmittance spectra of ITO and DMSO treated PEDOT:PSS films with different layers. The transmittance measured in this study excludes the absorption of the glass substrate since the glass substrates we used for PEDOT:PSS coating were different from those employed for commercial ITO deposition. The transmittance at 550 nm is 96%, 93% and 89% for single layer, double layers and triple layers, respectively. This result indicates that the thick film results in transmission loss.

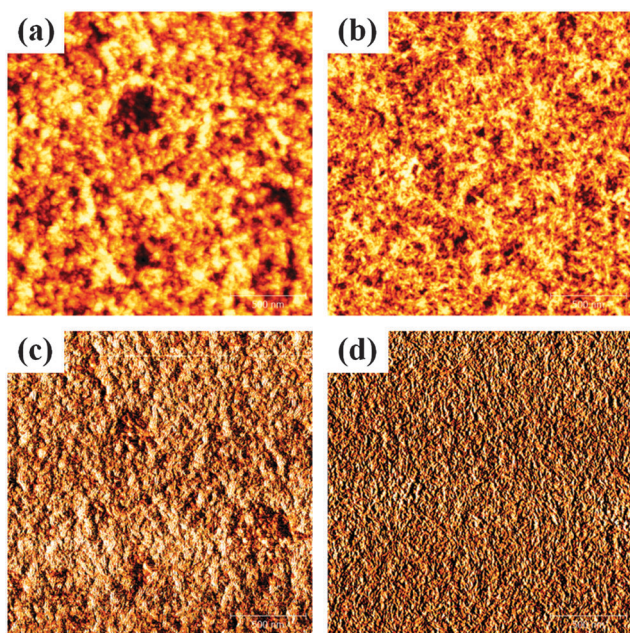


Fig. 5 AFM images of PEDOT:PSS films before (a and c) and after (b and d) the DMSO post-treatment. (a) and (b) are surface topography images while (c) and (d) are phase images. The dimension of these images is 2  $\mu\text{m} \times 2 \mu\text{m}$ .

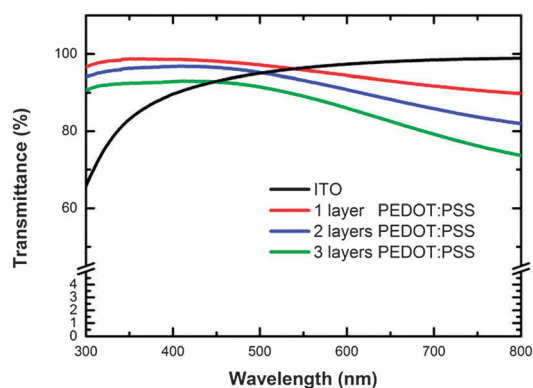


Fig. 7 Transmittance spectra of ITO and PEDOT:PSS film with different layers. The sheet resistance of the ITO is 95  $\Omega \square^{-1}$ .

The sheet resistance and transmittance of the double layer sample are comparable to those of the ITO (transmittance 96% and sheet resistance  $95 \Omega \square^{-1}$ ) we used for comparison in this study.

In order to align LC molecules on the PEDOT:PSS film, the rubbing process was employed. Several materials such as velvet cloth and silicon rubber sheet have been adopted in the rubbing process. In our case, we used a polyester cloth to generate the oriented nanoscale-groove structure on the surface of the PEDOT:PSS layer. The surface relief structures of the rubbed PEDOT:PSS films captured by AFM are shown in Fig. 8. The orientation of induced grooves is uniformly aligned along the rubbing direction and the depth of the grooves ranges from a few nanometers to 10 nm. Previous studies have shown that the surface topography of the substrate and the chemical reaction between LC molecules and the alignment layer play crucial roles in the alignment mechanism.<sup>39,40</sup> In this study, we consider that it is the grooved surface of the PEDOT:PSS film and the aromatic rings of PSS which account for the LC alignment.

Fig. 9(a) and (b) show POM images of LC cells fabricated using the rubbed highly conductive PEDOT:PSS films with and without the applied external field, respectively. These images were taken in normally black mode. In normally black mode, it would be easy to observe light leakage spots if the TN configuration achieved by the rubbed PEDOT:PSS films has some defects. In these pictures, uniform dark and bright states were obtained which indicates that the rubbed highly conductive PEDOT:PSS films could align LC molecules well and it would not generate optically observable flaws in the bright state.

In order to investigate the electro-optical properties of the LC cells using the rubbed highly conductive PEDOT:PSS as both the electrode and alignment layer,  $V$ - $T$  characteristics and response times of these samples were measured. Fig. 10 shows the normalized transmittance of TN LC cells fabricated using glass/PEDOT:PSS and glass/ITO/PI under applied AC square wave voltage with the amplitude varying from 0 to 4 V. Measured results indicate that the  $V$ - $T$  characteristics of cells constructed by PEDOT:PSS were similar to those of the samples fabricated by PI coated ITO glass. In comparison with the  $V$ - $T$  curve of the sample using ITO and PI, the  $V$ - $T$  curve of the sample using

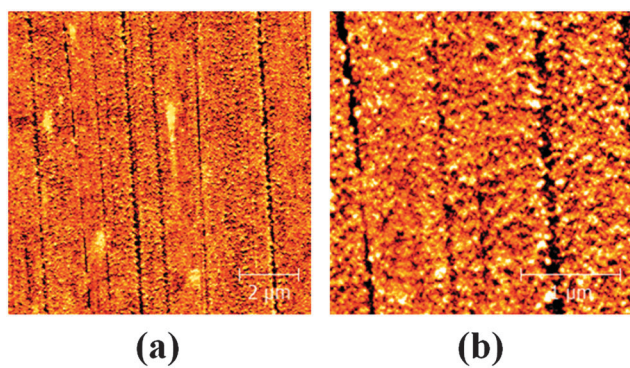


Fig. 8 Surface topography of the rubbed highly conductive PEDOT:PSS films. The dimensions of these images are (a)  $10 \mu\text{m} \times 10 \mu\text{m}$  and (b)  $3 \mu\text{m} \times 3 \mu\text{m}$ .

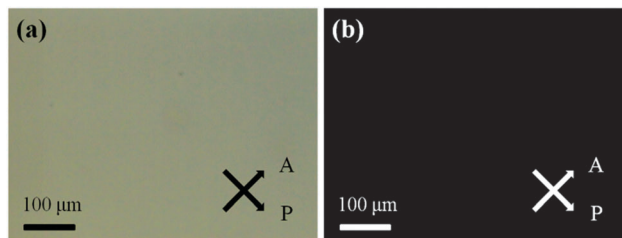


Fig. 9 POM images of TN LC cells fabricated by the rubbed highly conductive PEDOT:PSS films in normally black mode (a) with and (b) without the applied external field.

PEDOT:PSS shifts to higher voltage slightly. This is due to the difference in conductivity between PEDOT:PSS and ITO, which leads to a slight voltage drop on the PEDOT:PSS electrode. The threshold voltage and driving voltage are defined as the voltage corresponding to 90% and 10% of the initial transmittance, respectively. The measured threshold and driving voltage of the sample using PEDOT:PSS were 1.65 V and 2.67 V, which were very close to the results of the sample fabricated by ITO and PI (1.55 V and 2.55 V).

Fig. 11 shows the response time characteristics of TN LC cells fabricated using glass/PEDOT:PSS and glass/ITO/PI under applied AC square wave voltage with an amplitude of 6 V. Rise time and decay time are defined as the time interval between 90% and 10% of the initial transmittance after the external voltage was applied and removed, respectively. Response time is defined as the sum of rise time and decay time. The measured rise time and decay time of the samples fabricated using PEDOT:PSS were 3.36 ms and 15.57 ms respectively, which were faster than those of the samples using ITO and PI (4.02 ms and 25.49 ms). The LC cell constructed by PEDOT:PSS shows a faster response time, especially in the decay time. One reason accounting for this phenomenon might be the lack of the PI layer. When the applied voltage was removed, some induced dipole moments in the PI layer generated by the external electric field increase the time for LC molecules to rotate back to the twist state. To sum up, threshold voltage and

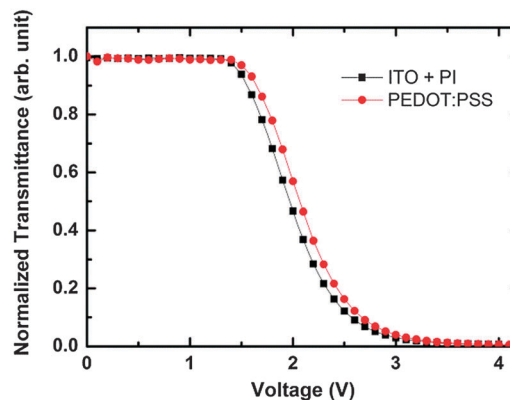


Fig. 10 Transmittance of TN LC cells fabricated by the rubbed highly conductive PEDOT:PSS on glass and polyimide on ITO glass under applied AC square wave voltage.

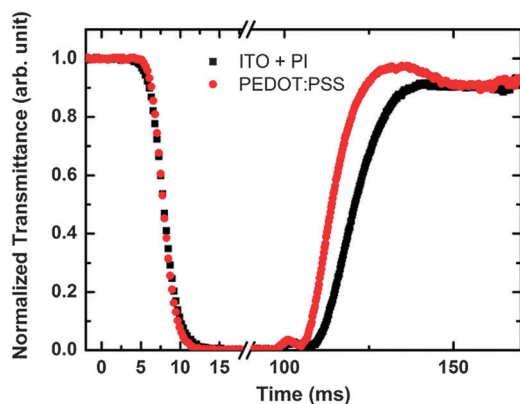


Fig. 11 Response time characteristics of TN LC cells fabricated by the rubbed highly conductive PEDOT:PSS on glass and polyimide on ITO glass.

response time are key factors which correspond to the power consumption and the image quality of LC devices in the LCD industry, respectively. The measured results show that PEDOT:PSS used as both a transparent electrode and an alignment layer in LC cells possesses low power consumption and fast response characteristics as traditional LC devices and could further expand LC devices to the flexible electronic field.

## Conclusion

In summary, a simple and effective method to enhance the conductivity of PEDOT:PSS thin films by four orders of magnitude is demonstrated. The conductivity of the pristine PEDOT:PSS film increased drastically from 0.7 to  $1185 \text{ S cm}^{-1}$  after post-treatment with 2% of DI water doped DMSO. The removal of the insulating PSS together with the re-ordering and conformation changes of the PEDOT and PSS chains are the prime reasons for the conductivity enhancement observed in this study. Uniform LC alignment on the highly conductive PEDOT:PSS film was achieved by using the rubbing technique. The electro-optical properties of TN LC cells fabricated by the rubbed highly conductive PEDOT:PSS film show comparable results relative to those fabricated by ITO and PI. This work indicates that the highly conductive PEDOT:PSS film is a promising material as both the transparent electrode and the alignment layer to replace ITO for ITO-free and flexible LC displays.

## Acknowledgements

One of us (C.Y.C.) acknowledges the support from National Taiwan University, Ministry of Science and Technology, and Ministry of Education of the Republic of China. The authors would like to thank Mr Yen-Cheng Chao for his helpful assistance in AFM measurements.

## Notes and references

- 1 M. Ohe and K. Kondo, *Appl. Phys. Lett.*, 1995, **67**(26), 3895.
- 2 Y.-J. Lee, Y.-K. Kim, S. I. Jo, J. S. Gwag, C.-J. Yu and J.-H. Kim, *Opt. Express*, 2009, **17**(12), 10298.

- 3 S. H. Lee, S. L. Lee and H. Y. Kim, *Appl. Phys. Lett.*, 1998, **73**(20), 2881.
- 4 D. R. Cairns, R. P. Witte, D. K. Sparacin, S. M. Sachsman, D. C. Paine, G. P. Crawford and R. R. Newton, *Appl. Phys. Lett.*, 2000, **76**(11), 1425.
- 5 C. S. Tao, J. Jiang and M. Tao, *Sol. Energy Mater. Sol. Cells*, 2011, **95**, 3176.
- 6 A. Chipman, *Nature*, 2007, **449**, 131.
- 7 K. Saxena, V. K. Jain and D. S. Mehta, *Opt. Mater.*, 2009, **32**, 221.
- 8 J. M. Phillips, R. J. Cava, G. A. Thomas, S. A. Carter, J. Kwo, T. Siegrist, J. J. Krajewski, J. H. Marshall, W. F. Peck and D. H. Rapkine, *Appl. Phys. Lett.*, 1995, **67**(15), 2246.
- 9 Z. C. Wu, Z. H. Chen, X. Du, J. M. Logan, J. Sippel, M. Nikolou, K. Kamaras, J. R. Reynolds, D. B. Tanner, A. F. Hebard and A. G. Rinzler, *Science*, 2004, **305**, 1273.
- 10 M. Zhang, S. L. Fang, A. A. Zakhidov, S. B. Lee, A. E. Aliev, C. D. Williams, K. R. Atkinson and R. H. Baughman, *Science*, 2005, **309**, 1215.
- 11 G. Gruner, *J. Mater. Chem.*, 2006, **16**, 3533.
- 12 P. Joshi, L. F. Zhang, Q. L. Chen, D. Galipeau, H. Fong and Q. Q. Qiao, *ACS Appl. Mater. Interfaces*, 2010, **2**(12), 3572.
- 13 J.-Y. Lee, S. T. Connor, Y. Cui and P. Peumans, *Nano Lett.*, 2008, **8**(2), 689.
- 14 P.-C. Hsu, S. Wang, H. Wu, V. K. Narasimhan, D. S. Kong, H. R. Lee and Y. Cui, *Nat. Commun.*, 2013, **4**, 2522.
- 15 J. Meiss, M. K. Riede and K. Leo, *Appl. Phys. Lett.*, 2009, **94**, 013303.
- 16 V. C. Tung, L.-M. Chen, M. J. Allen, J. K. Wassei, K. Nelson, R. B. Kaner and Y. Yang, *Nano Lett.*, 2009, **9**(5), 194.
- 17 X. G. Mei and J. Y. Ouyang, *Carbon*, 2011, **49**, 5389.
- 18 Y. J. Xia, K. Sun and J. Y. Ouyang, *Energy Environ. Sci.*, 2012, **5**, 5325.
- 19 J. E. Yoo, K. S. Lee, A. Garcia, J. Tarver, E. D. Gomez, K. Baldwin, Y. M. Sun, H. Meng, T.-Q. Nguyen and Y.-L. Loo, *Proc. Natl. Acad. Sci. U. S. A.*, 2010, **107**(13), 5712.
- 20 S.-I. Na, S.-S. Kim, J. Jo and D.-Y. Kim, *Adv. Mater.*, 2008, **20**, 4061.
- 21 L. B. Groenendaal, F. Jonas, D. Freitag, H. Pielartzik and J. R. Reynolds, *Adv. Mater.*, 2000, **12**(7), 481.
- 22 Y. Cao, G. Yu, C. Zhang, R. Menon and A. J. Heeger, *Synth. Met.*, 1997, **87**, 171.
- 23 S. Kirchmeyer and K. Reuter, *J. Mater. Chem.*, 2005, **15**, 2077.
- 24 A. Laskarakis, P. G. Karagiannidis, D. Georgiou, D. M. Nikolaidou and S. Logothetidis, *Thin Solid Films*, 2013, **541**, 102.
- 25 C. Badre, L. Marquant, A. M. Alsayed and L. A. Hough, *Adv. Funct. Mater.*, 2012, **22**, 2723.
- 26 M. Reyes-Reyes, I. Cruz-Cruz and R. Lopez-Sandoval, *J. Phys. Chem. C*, 2010, **114**, 20220.
- 27 J. S. Huang, P. F. Miller, J. S. Wilson, A. J. de Mello, J. C. de Mello and D. D. C. Bradley, *Adv. Funct. Mater.*, 2005, **15**(2), 290.
- 28 K. Sun, Y. J. Xia and J. Y. Ouyang, *Sol. Energy Mater. Sol. Cells*, 2012, **97**, 89.
- 29 Y. H. Kim, C. Sachse, M. L. Machala, C. May, L. Muller-Meskamp and K. Leo, *Adv. Funct. Mater.*, 2011, **21**, 1076.

- 30 Y. J. Xia and J. Y. Ouyang, *Org. Electron.*, 2010, **11**, 1129.
- 31 Y. J. Xia, K. Sun and J. Y. Ouyang, *Adv. Mater.*, 2012, **24**, 2436.
- 32 S.-I. Na, G. Wang, S.-S. Kim, T.-W. Kim, S.-H. Oh, B.-K. Yu, T. Lee and D.-Y. Kim, *J. Mater. Chem.*, 2009, **19**, 9045.
- 33 Y.-H. Ha, N. Nikolov, S. K. Pollack, J. Mastrangelo, B. D. Martin and R. Shashidhar, *Adv. Funct. Mater.*, 2004, **14**(6), 615.
- 34 U. Lang, E. Muller, N. Naujoks and J. Dual, *Adv. Funct. Mater.*, 2009, **19**, 1215.
- 35 S. Garreau, G. Louarn, J. P. Buisson, G. Froyer and S. Lefrant, *Macromolecules*, 1999, **32**, 6807.
- 36 S. Garreau, J. L. Duvail and G. Louarn, *Synth. Met.*, 2001, **125**, 325.
- 37 J. Krajcovic, G. Cik, D. Vegh and F. Sersen, *Synth. Met.*, 1999, **105**, 79.
- 38 J. Y. Ouyang, C.-W. Chu, F.-C. Chen, Q. F. Xu and Y. Yang, *Adv. Funct. Mater.*, 2005, **15**(2), 203.
- 39 J. S. Gwag, J. Yi, J. H. Kwon, M. Yoneya and H. Yokoyama, *J. Appl. Polym. Sci.*, 2011, **119**, 325.
- 40 J. Hoogboom, T. Rasing, A. E. Rowan and R. J. M. Nolte, *J. Mater. Chem.*, 2006, **16**, 1305.

# Supramolecular Liquid-Crystal Gels Formed by Polyfluorene-Based $\pi$ -Conjugated Polymer for Switchable Anisotropic Scattering Device

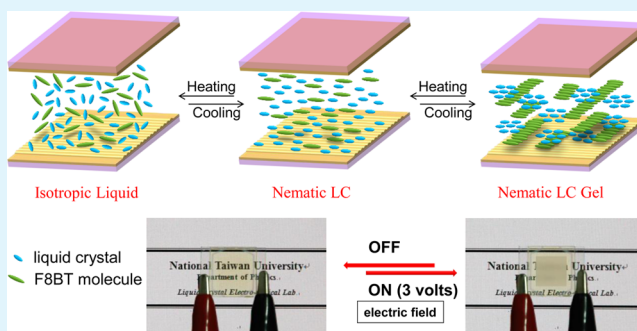
Jun-Wei Chen, Chiu-Chang Huang, and Chih-Yu Chao\*

Department of Physics, National Taiwan University, Taipei 10617, Taiwan, R.O.C.

## S Supporting Information

**ABSTRACT:** To overcome the problem of high driving voltage and low contrast ratio in the switchable scattering device of conventional liquid-crystal (LC) physical gel, a new type of supramolecular LC physical gel has been developed and fabricated through the fibrous self-assembly of the polyfluorene-based  $\pi$ -conjugated polymer, poly(9,9-dioctylfluorene-*alt*-benzothiadiazole) (F8BT), in nematic LC mixture E7. It was found that the rubbed interface between the LC molecules and polyimide layer can induce the LC physical gels to demonstrate fantastic light scattering characteristic. The gels with oriented self-assembled supramolecular structures exhibiting significant anisotropic light scattering in the main-chain direction of the F8BT molecules under an extremely low driving voltage (ca. 2.7 V) are reported for the first time. In addition, the contrast ratio can be reached exceeding 1000. In contrast to conventional LC physical gels, the large reduction of driving voltages of the supramolecular gel provides great possibility for application in various electro-optical devices such as tunable polarizers, transfective displays, and polarized light modulators.

**KEYWORDS:** anisotropic scattering, molecular self-assembly, liquid-crystal physical gels, electrically switchable devices, supramolecular structures, polyfluorene-based  $\pi$ -conjugated polymer



## 1. INTRODUCTION

Organic gelator molecules have attracted significant attention for the ability to form physical network structure through self-assembly in solvents.<sup>1–9</sup> The non-covalent interactions like hydrogen-bonding,  $\pi$ - $\pi$  stacking, and van der Waals force induce the formation of fibrous aggregates of the organic gelators. In recent years, the thermal-reversible fibrous network assembling in LCs leads to the construction of physical gels,<sup>10–16</sup> which have been developed as soft functional materials. The functional gel materials have been widely used in various electro-optical devices, such as LC semiconductors with high mobility,<sup>17,18</sup> fast-response switching in twisted nematic cells,<sup>19–21</sup> stabilization of the orientation of ferroelectric LCs,<sup>22</sup> etc. In particular, switchable scattering devices based on the LC physical gels have attracted more and more interests for their potential to apply to a new mode of display.<sup>23–28</sup> However, in these gels, high driving voltages of about 40 V are still needed to switch the bright and dark states. And the contrast ratios are also not high enough for the use of displays. In this paper, we report for the first time that a supramolecular LC gel can be formed by the use of polyfluorene-based  $\pi$ -conjugated polymer as gelator and the gel demonstrates fantastic electro-optical properties. In contrast to conventional LC physical gels, the supramolecular gel possesses extremely low driving voltage less than 3 V which provides great applications in various electro-optical devices.

The  $\pi$ -conjugated gelator molecule used in this experiment is poly(9,9-dioctylfluorene-*alt*-benzothiadiazole) (F8BT). The electro-optical properties of the F8BT molecule as thin films have been studied in previous experiments in detail.<sup>29–31</sup> The F8BT molecule is one kind of the polyfluorene derivatives which have been developed as the active organic materials in the electro-optical device, such as polymer light-emitting diodes (PLEDs) and polymer field effect transistors (PFETs) with highly conducting properties caused by the  $\pi$ -conjugated chains.<sup>32–36</sup> Besides, many researchers found that the polyfluorene derivatives can gel a lot of organic solvents through the fibrous self-assembly of polymers induced by the  $\pi$ - $\pi$  stacking interactions between molecules.<sup>37–39</sup> Until now, however, only few studies have been investigated on the self-assembled behavior of polyfluorene derivatives in LCs. Here we first report that the LC mixture E7 can be gelled by the polyfluorene derivatives–F8BT polymer. In addition, the supramolecular anisotropic structures have been observed in an LC cell with anti-parallel alignment layer after the formation of the LC gels through fibrous self-assembly of the  $\pi$ -conjugated gelator F8BT. The presence of oriented polymer network in LCs makes the supramolecular  $\pi$ -conjugated gel exhibit extremely anisotropic scattering and high contrast ratio

Received: January 24, 2014

Accepted: April 11, 2014

Published: April 11, 2014



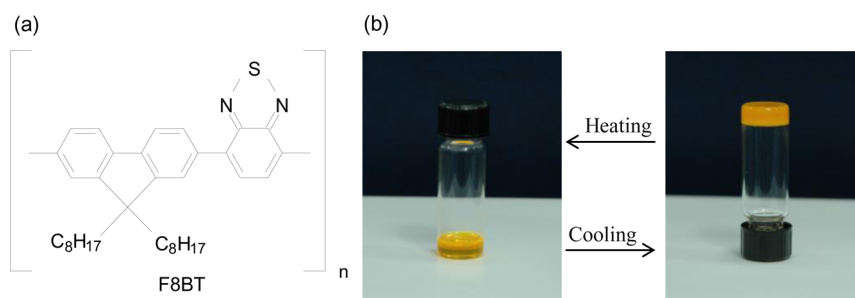


**Figure 1.** (a) Chemical structure of the polyfluorene-based  $\pi$ -conjugated polymer F8BT. (b) Photographs of the formation of LC gel with 1.0 wt % F8BT in E7. The pictures show the thermal reversibility which was examined by repeated heating–cooling processes.

under an ultra-low driving voltage (only 2.7 V) compared to the conventional gels formed by low-molecular-weight gelators. The unique properties of the polyfluorene-based supramolecular anisotropic LC gel provide the possibility to develop a novel electro-optical material for promising applications in switchable devices.

## 2. EXPERIMENTAL SECTION

**2.1. Preparation of Supramolecular LC Gels.** In this study, the nematic LC E7 (clearing point about 51 °C) and the polyfluorene-based  $\pi$ -conjugated polymer F8BT (average  $M_n$  10,000–20,000) were used to construct the supramolecular LC physical gels. They were purchased from Fusol material and Sigma-Aldrich, respectively. The chemical structure of F8BT is shown in Figure 1a. The LC host E7 was used in our experiments due to the F8BT polymer had good solubility and stability in it. The nematic LC E7 is a mixture which consists of four kinds of basic LC molecules: [1,1'-biphenyl],4-carbonitrile,4'-pentyl, [1,1'-biphenyl],4-carbonitrile,4'-heptyl, [1,1'-biphenyl],4-carbonitrile,4'-octyloxy, and [1,1',4'-1''-terphenyl],4-carbonitrile,4''-pentyl with the percentages of 51, 25, 16, and 8, respectively.

To prepare the supramolecular LC physical gels, at first, a small amount of F8BT (0.1–1.6 wt %) was adding into E7 LCs in glass bottles. Then these materials were uniformly mixed by stirring and gently heating on a hot plate. In the beginning, the LC mixtures of F8BT and E7 displayed an opaque state in the room temperature. When the mixtures were heated to the temperature of about 60 °C, which is higher than the clearing point of E7, the mixtures became transparent for being an isotropic liquid. To make sure the F8BT polymers can be well dispersed in E7, the mixtures were further heated at 90 °C for 3 h. And then the mixtures were cooled down slowly at a rate of 5 °C min<sup>-1</sup>. As the temperature cooled down to room temperature, the mixtures became opaque again and formed the supramolecular LC gels. The formation of the gel can be validated by the loss of the ability to flow under the influence of gravity as shown in Figure 1b. Figure 1b shows the photographs of the LC gel with the concentration of 1.0 wt % F8BT in E7. The occurrence of the thermal reversibility reflects the reason for the construction of the gel from the non-covalent network.

**2.2. Examination of Phase Transition Behavior.** To understand the phase transition behavior of the supramolecular LC gels, the E7 with different concentrations of F8BT polymers were examined. The sol–gel transition temperatures ( $T_{\text{sol-gel}}$ ) of F8BT and the isotropic–nematic transition temperatures ( $T_{\text{iso-ne}}$ ) of E7 were determined by differential scanning calorimetry (DSC) measurements and polarized optical microscope (POM) observations in the cooling process at a rate of 5 °C min<sup>-1</sup>. The DSC measurements were performed on a Perkin Elmer Pyris 6 DSC instrument. By confirming that the exothermic peaks occur in the DSC data, the transition temperatures of  $T_{\text{iso-ne}}$  and  $T_{\text{sol-gel}}$  can be obtained. To observe the images of POM, the gels containing different concentrations of F8BT were injected into 9  $\mu\text{m}$  thickness glass sandwich cells having anti-parallel rubbed polyimide films in isotropic liquid state. And the POM observations of cells were conducted using Olympus BX51 equipped with a hot stage.

As the temperature decreases, the transition temperature of  $T_{\text{iso-ne}}$  and  $T_{\text{sol-gel}}$  can also be observed through the POM.

**2.3. Observation of the Self-Assembled Structures of LC Gels on the Rubbed and Unrubbed Interfaces.** The gels containing different concentrations of F8BT were prepared as described in Section 2.1. Then the gels were injected into the 9  $\mu\text{m}$  thickness glass sandwich cells with anti-parallel rubbed polyimide films or unrubbed polyimide films. To confirm the mixing uniformity, the gels were heated to isotropic liquid state and then injected into the cells. Subsequently, the cells were cooled down slowly to room temperature at a rate of 5 °C min<sup>-1</sup>, and the supramolecular LC gels were formed in the cells. To observe the structure of the gels in the cells, the dark-field mode of Olympus BX51 was conducted. For further realizing the main-chain direction of the F8BT polymer in the cells, the polarized PL spectra (excitation light  $\lambda_{\text{ex}} = 430 \text{ nm}$ ) were measured through the instrument of Edinburgh FS 920. By adjusting the polarization of polarizer between the cell and the detector to be parallel or perpendicular with the rubbing direction of the cell, the polarized PL spectra can be obtained.

**2.4. Electro-Optical Measurements of Supramolecular Anisotropic Gels.** For researching the electro-optical properties of the supramolecular LC gels, the gels were injected into the 9  $\mu\text{m}$  thickness ITO (indium tin oxide) glass cell with anti-parallel rubbed polyimide films or unrubbed polyimide films by the method described in Section 2.3. To demonstrate the property of anisotropic scattering of the LC gel in the cell with rubbed surface, the LC cell was placed in front of a polarized LC display. By providing a low voltage (ca. 3 V), the electrode area of the LC cell presented an obvious scattering. And the detailed electro-optical properties of the supramolecular LC gels are further measured by our experiment system shown in Figure 2.

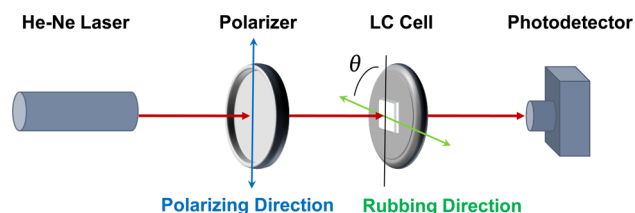


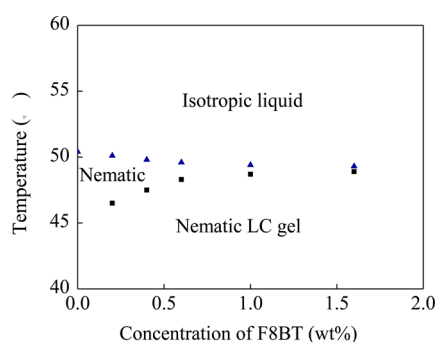
**Figure 2.** Illustration that shows the setup of the electro-optical measurement system.  $\theta$  is defined as the rotation angle between the polarizing direction of polarizer and the rubbing direction of the LC cell.

The system is composed of a He–Ne laser, linear polarizer, LC cell, and the photodetector. An unpolarized He–Ne (632.8 nm) laser was used as an incident light source. To verify the property of directional scattering of the supramolecular LC gel, the polarizer mounted in a rotatable holder was placed between the He–Ne laser and the LC cell. An AC field (1 kHz, square wave) was applied to the cells by the function generator which was controlled by a computer with LabView programming. Then the transmittances under various applied voltages were recorded by the photodetector. The driving voltage was determined to be the voltage required for reaching 90% transmittance

relative to the empty cell as background. And the data of rise time and the decay time were determined by measuring the response times needed for varying the transmittances 100–10% and 0–90% in the electric field (5 V) on and off, respectively. The transmittances in various rotation angles  $\theta$  between the polarization of polarizer and the rubbing direction of the cell were recorded by rotating the polarizer. In addition, the broad transmittance spectra in the electric field on and off for two directions were measured by the SD1200-LS-HA system.

### 3. RESULTS AND DISCUSSION

**3.1. LC Gel Preparation and Its Phase Transition Behavior.** After the formation of supramolecular LC gels through the steps described previously, the phase behaviors of the gels were further researched. Figure 3 shows the phase



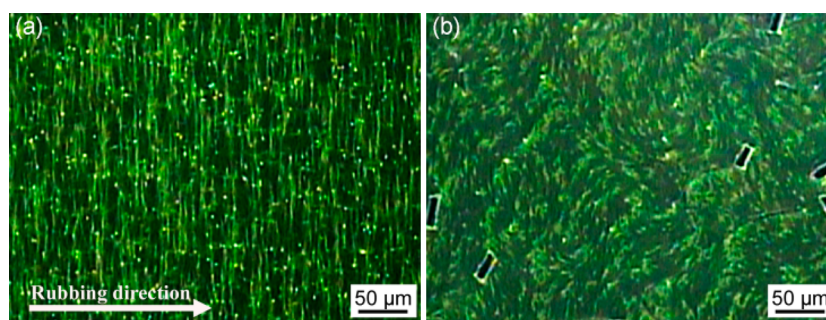
**Figure 3.** Phase diagram of the mixtures of E7 and F8BT. The mixtures with different concentrations of 0.2, 0.4, 0.6, 1.0, and 1.6 wt % F8BT were prepared. The  $T_{\text{sol-gel}}$  of F8BT and  $T_{\text{iso-ne}}$  of E7 are represented by ■ and ▲, respectively.

diagram of the supramolecular LC gels with different concentrations of F8BT which was determined by the POM observations and DSC measurements (some representative DSC data are shown in Supporting Information Figure S1). In our experiments, the gels with the concentrations of F8BT below 1.6 wt % exhibit three states of isotropic liquid, nematic, and nematic LC gel in the phase diagram. And the mixtures undergo the isotropic–nematic transition of E7 first and then sol–gel transition of F8BT upon cooling. This finding implies that it is possible to align the F8BT molecules and form oriented molecular network structures through the template effect of the aligned LC materials.

**3.2. Observation of Fibrous Structures of the Gels.** To confirm this assumption, the gels with different concentrations of F8BT were filled into a 9  $\mu\text{m}$  empty LC cells with anti-parallel rubbed alignment layers in isotropic liquid state. After

the cooling processes described in the experiment part, we found that the anisotropic fibrous structures were formed in the LC cells through the observations with dark-field optical microscope. Figure 4a shows the dark-field optical picture of the cell with the gel containing 1.0 wt % of F8BT. The green self-assembled F8BT fibers perpendicular to the rubbing direction of the cell were observed in this figure. Figure 4b shows the optical picture of the cell (without rubbing treatment) with the gel containing 1.0 wt % of F8BT; the random polymer network can be observed. These results are supported by the phase diagram shown in Figure 3. It indicates that the anisotropic fibrous aggregates of the gelator F8BT can be formed through the use of rubbed surface, since the  $T_{\text{iso-ne}}$  is higher than  $T_{\text{sol-gel}}$ . The template effect of the aligned nematic LCs is a key role to induce the formation of oriented fibrous aggregates of F8BT. Without the template effect (no rubbing treatment for the cells), there are only the random polymer networks formed in the cells.

There have been a number of studies that have investigated the properties of F8BT polymer, which reveal that the F8BT molecules with uniaxial alignment result in polarized photoluminescence (PL).<sup>31,40</sup> Therefore, to confirm the orientation of F8BT molecules in the cell with rubbed surface, the polarized PL spectra of the gels containing different concentrations of the gelator F8BT were measured. The polarized PL spectra were obtained by setting a polarizer, which was inserted between the cell and detector, with the polarization to be parallel or perpendicular in the rubbing direction of the cell. Figure 5a shows the PL emission spectra ( $\lambda_{\text{ex}} = 430 \text{ nm}$ ) of the LC gel containing 0.1 wt % F8BT, and the measured PL polarization ratio of parallel to perpendicular intensity at 540 nm is over 3. Figure 5b shows the PL polarization ratios with different F8BT concentrations between 0.1 and 1.6 wt %. For the LC cells with the gels containing F8BT below 1 wt %, high PL polarization ratios were observed. These findings reflect the degree of alignment of fibrous F8BT polymer network to a great extent. The higher PL polarization ratio was obtained in cell with a lower concentration of F8BT. Besides, the stronger PL signal was recorded when the polarization of polarizer was parallel to the rubbing direction of the cells. The result shows that the main-chain direction of F8BT molecules should align with the rubbing direction of cell. Supporting Information Figure S2 shows the polarized PL spectra for samples prepared in cells without rubbing treatment. It can be seen that the polarized PL spectra in two directions are almost the same. And no obvious tendency is found as the concentration of F8BT increases. It indicates that the F8BT



**Figure 4.** Dark-field optical pictures of F8BT/E7 gels containing 1.0 wt % of F8BT in E7 LCs in the cell (a) with anti-parallel rubbed alignment layer in which the anisotropic self-assembled fibers of F8BT was shown and (b) without rubbing treatment in which the polymer network of F8BT was found in the cell.

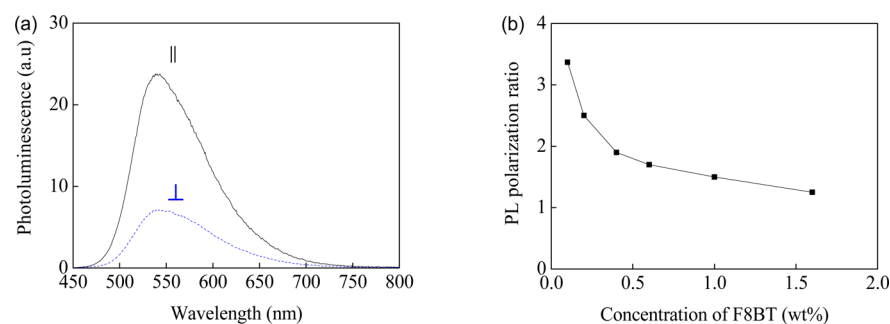


**Figure 5.** (a) Polarized PL spectra of a LC gel containing 0.1 wt % F8BT in E7. The solid and dashed curves denote the PL spectrum as the polarizing direction of polarizer was parallel and perpendicular to the rubbing direction of the cell, respectively. (b) The polarization ratios of LC gels with different concentrations of 0.1, 0.2, 0.4, 0.6, 1.0, and 1.6 wt % F8BT.

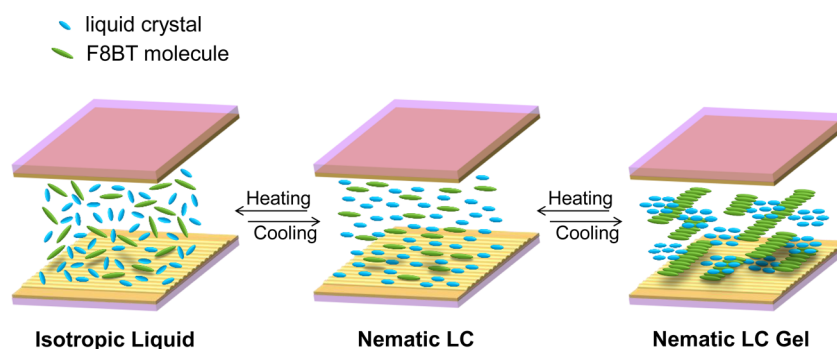


**Figure 6.** Schematics of the formation model of anisotropic  $\pi$ -conjugated F8BT fibers (shown as fibrous aggregates of green F8BT molecules) in three states of isotropic liquid, nematic LC, and nematic LC gel. In the cooling process, the F8BT/E7 mixture would undergo isotropic–nematic transition of E7 and then sol–gel transition of F8BT. With the  $\pi$ – $\pi$  stacking interaction between the aligned F8BT molecules, anisotropic fibrous polymer networks are formed through oriented self-assembly.

molecules would align randomly in the cells without rubbing treatment.

According to the measurements of polarized PL spectrum and the results of OM observations, we can build up the formation model of anisotropic  $\pi$ -conjugated F8BT fibers which is shown in Figure 6. In the beginning, the mixture of E7 and F8BT is in a state of isotropic liquid that the F8BT molecules are randomly dispersed in the LC host E7 after being injected into the cell and heated to the temperature higher than  $T_{\text{iso-ne}}$ . Then, as the cell is cooled down slowly to the temperature below  $T_{\text{iso-ne}}$ , the F8BT molecules can be aligned to the rubbing direction of the LC cell through the template effect of E7 LCs in the nematic LC state. Subsequently, as the temperature keeps cooling down to  $T_{\text{sol-gel}}$ , the  $\pi$ – $\pi$  stacking interactions between the main chains of F8BT molecules lead to the formation of nematic LC gel through the self-assembly of the anisotropic F8BT fibers with the growth direction perpendicular to the rubbing direction of the LC cell.<sup>29</sup> And we found the fibrous structure is thermal-reversible, which means the anisotropic fibers would disappear as the gel is heated to the temperature higher than the  $T_{\text{sol-gel}}$  and become isotropic liquid again if the temperature is further heated to the temperature higher than the  $T_{\text{iso-ne}}$ .

The self-assembled behavior of the gelator F8BT is similar to the previous results reported by Kato et al.; low-molecular-weight  $\pi$ -conjugated gelator can form oriented fibrous aggregates which are perpendicular to the rubbing direction through  $\pi$ – $\pi$  stacking interaction.<sup>41,42</sup> To examine the existence of  $\pi$ – $\pi$  stacking interactions between F8BT polymers, we measure the  $^1\text{H}$  NMR spectroscopy of F8BT polymers in  $\text{CDCl}_3$  (10 mg/1 mL) with different temperatures of 248, 273,

and 298 K (see Supporting Information Figure S3). It shows that, as the temperature decreases, the aromatic proton signals become not well-resolved. That indicates the stronger  $\pi$ – $\pi$  stacking interactions occur as the temperature decreases.<sup>43</sup> These results here provide the evidence for the existence of the  $\pi$ – $\pi$  stacking interactions between F8BT polymers. It is worth emphasizing that although the polyfluorene-based polymer F8BT is a high-molecular-weight molecule with a long  $\pi$ -conjugated chain, the F8BT polymers can also be aligned by the template effect of the oriented nematic LCs.

**3.3. Electrically Switchable Anisotropic Light Scattering.** With the formation of oriented fibrous structure in the cell with rubbing treatment, we found such a supramolecular LC gel demonstrates an extremely anisotropic light scattering state by providing an electric field. Figure 7 illustrates the photographs of the cell with the LC gel containing 0.2 wt % F8BT and the mechanism of anisotropic scattering in the field-off and field-on states. These photographs were taken by using a polarized LC display screen as the light source, and its polarization was arranged to be parallel with the rubbing direction of the cell. And these pictures were obtained in the distance about 1 cm between cell and screen. The gel exhibits transparent state when the electric field is off. And when the electric field turns on, the gel would switch to the anisotropic scattering state. The state makes the light with the polarization axis parallel to the rubbing direction of the cell extremely scatter. Therefore, the gel presents an opaque state on the square electrode area of the cell. And when the electric field turns off, the LC gel is switched back to the transparent state again. It is remarkable to note that the driving voltage required to produce such electro-optical switching from a transparent state to an anisotropic scattering

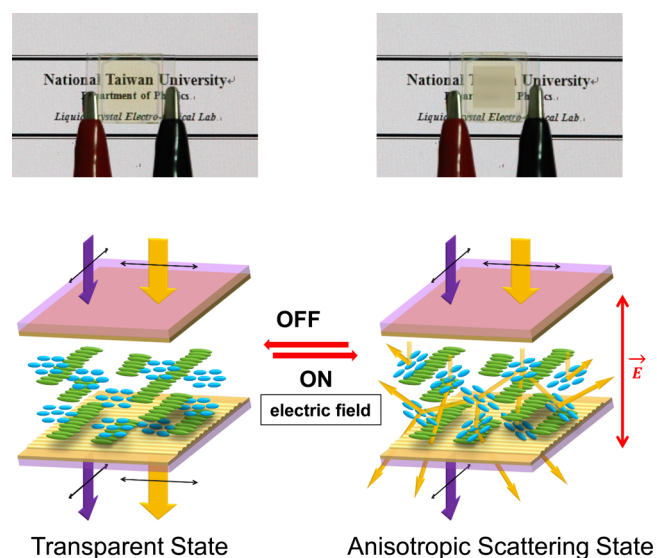


**Figure 7.** Schematics illustrating the anisotropic scattering mechanism and the corresponding photographs of the cell with the 0.2 wt % F8BT supramolecular LC gel in the electric field-off and field-on states, respectively. The two states can be electrically switched by a low applied voltage, less than 3 V.

state is extremely low, less than 3 V. We consider the reason leading to low operating voltages should be due to the presence of  $\pi$ -electrons. The  $\pi$ -electrons may play as a kind of radical here, since the aromatic rings in the conjugated polymer have a high  $\pi$ -electron delocalization degree.<sup>44</sup> After the formation of conjugated network through the  $\pi$ -stacking interactions between F8BT molecules,  $\pi$ -electrons would obtain a higher delocalization degree.<sup>45</sup> Therefore, we suggest that these  $\pi$ -electrons could rapidly redistribute around the conjugated network and form localized electric fields which can efficiently drive LC molecules in much lower operating voltages. Through the utility of polyfluorene-based  $\pi$ -conjugated polymer F8BT and rubbed surface, the supramolecular LC gel shows the unique property of low driving voltage and anisotropic scattering, which are not found in the conventional LC gel formed by the oriented self-assembly of low-molecular-weight gelator.<sup>10,41,42,46</sup>

Here we propose a model to explain the anisotropic scattering mechanism of the supramolecular LC gel. In the absence of electric field, the supramolecular LC gel exhibits the transparent state because the LCs present a monodomain with orientation aligned to the rubbing direction of the cell. And then, when the electric field turns on, the LCs are forced to align to the direction of electric field. Meanwhile, the LC molecules are still attracted by the  $\pi$ - $\pi$  interactions from the oriented fibrous aggregates of the F8BT polymer. The

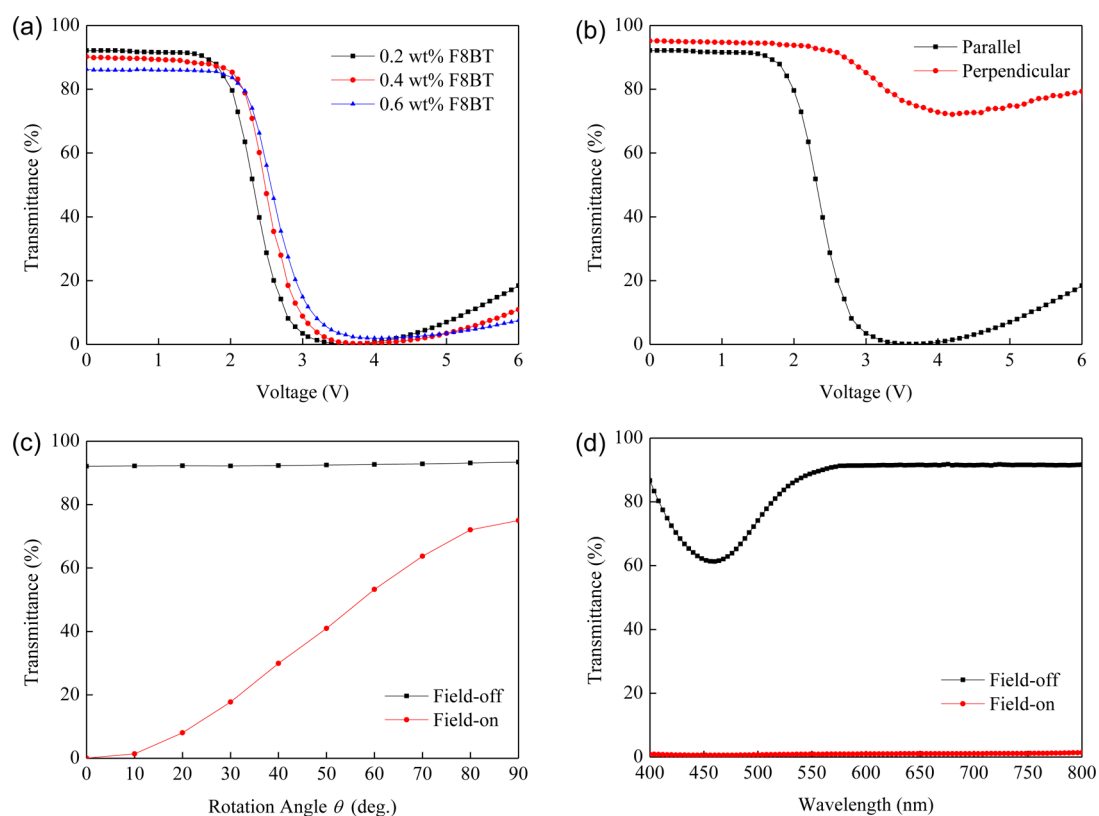


**Figure 8.** (a) Transmittance–voltage curves of the supramolecular LC gels with 0.2, 0.4, and 0.6 wt % of F8BT in a 9  $\mu\text{m}$  thick LC cell with anti-parallel rubbing treatment. The transmittances were recorded in the rubbing direction of the cell parallel to the polarization direction of the polarizer. (b) Comparison of the transmittance–voltage curves of 0.2 wt % F8BT/E7 gel with the rubbing direction of the cell parallel and perpendicular to the polarization direction of the polarizer. (c) The transmittance of 0.2 wt % F8BT supramolecular LC gel at the field-off (0 V) and field-on (3.6 V) states in different rotation angles between the polarization direction of the polarizer and the rubbing direction of the cell. (d) The transmittance spectrum of 0.2 wt % F8BT LC gel in the wavelength range from 400 to 800 nm. The transmittances were recorded at the polarization direction of the polarizer parallel to the rubbing direction of the cell in the field-off (0 V) and field-on (3.6 V) states.

competition of two forces induces the transformation from uniform monodomain to multi-domains which align to the main-chain direction of F8BT polymer in the plane parallel to the rubbing direction. With the formation of oriented LC multi-domains, the supramolecular LC physical gel demonstrates the result of anisotropic light scattering. And the LC multi-domains would reverse to the monodomain again as electric field turns off.

**3.4. Electro-Optical Properties of the Gels.** The electro-optical properties of the LC gels were examined by the measurement system shown in Figure 2. The LC cells filled by the gels with different concentrations of the gelator F8BT through the fabrication process as described in Experimental Section were prepared. Figure 8a shows the voltage–transmittance ( $V$ – $T$ ) curves of the LC gels with different concentrations (0.2, 0.4, and 0.6 wt %) of the gelator F8BT. The parallel transmittance ( $T_{\parallel}$ ) was recorded as the polarization direction of polarizer was set to be parallel with the rubbing direction of cell. As the electric field is off, the gel possesses the highest transmission state. When the electric field turns on, the transmittance starts to decrease due to the light scattering caused by the formation of multi-domains. As the driving voltage increases, the size of LC multi-domains becomes smaller and thus the transmittance further decreases. The transmittance reaches minimum as the size of LC multi-domains approaches the wavelength of visible light. But if the applied voltage continues to increase, the size of LC multi-domains would become larger and gradually transfer to monodomain, since the electric force is dominant as the driving further voltage increases over 4.5 V (as shown in Figure 8). Therefore, the transmittance starts to increase. In addition, the  $V$ – $T$  curves of the supramolecular LC gel are influenced by the concentration of the gelator F8BT.

For the lower concentration, the higher transmittance in the off state and lower driving voltage are obtained for little light absorption and faster response caused by the effect of higher ratio of LCs, respectively. The electro-optical properties of the supramolecular LC gels with different concentrations of the gelator F8BT are shown in Table 1. In our experiments, the LC

**Table 1. Electro-Optical Properties of the Supramolecular LC Gels with Different Concentrations of the F8BT Gelator**

concentration of F8BT (wt %)	driving voltage (V)	maximum contrast ratio	maximum polarization efficiency
0.2	2.7	1170	860
0.4	2.9	355	264
0.6	3.2	44	32

gel containing 0.2 wt % F8BT polymer presents the best performance of anisotropic scattering. The transmittance is as high as 92% when the electric field is off. Then when the electric field turns on, the gel exhibits anisotropic light scattering state at the driving voltage of only about 2.7 V. And the contrast ratio can be achieved to exceed over 1000 at 3.6 V. But for the gel with concentration of 0.1 wt % of F8BT, no obvious scattering is observed. We speculate the reason why the LC gel with 0.2 wt % F8BT can exhibit better electro-optical properties could be due to the size of the LC multi-domain being most suitable for the scattering of the visible light. To further realize the anisotropic scattering properties of the supramolecular LC gel, the perpendicular transmittances ( $T_{\perp}$ ) were measured by modulating the polarization direction

of polarizer to be perpendicular with the rubbing direction of the cell. Figure 8b shows the  $V$ – $T$  curves of the LC gel with 0.2 wt % F8BT in parallel and perpendicular directions. Instead of the evident scattering occurred in the parallel direction, only slight scattering was observed as the light polarization perpendicular with the rubbing direction of cell. Besides, the initial transmittance in the parallel direction is slightly lower than that in the perpendicular direction because of the higher absorption along with the main chain of the F8BT molecule. The polarization efficiencies of these supramolecular LC gels with different F8BT concentrations are also shown in Table 1. The polarizing efficiency (PE) is calculated as follows:

$$PE = (T_{\perp} - T_{\parallel}) / (T_{\perp} + T_{\parallel}) \quad (1)$$

The LC gel with 0.2 wt % F8BT demonstrates the best polarization efficiency at the voltage about 3.6 V. And the polarizing efficiency can be reached up to 860. The relationship between the transmittance and rotation angle was also investigated. The transmittance of the LC gels containing 0.2 wt % F8BT at the field-off (0 V) and field-on (3.6 V) states in a different rotation angle  $\theta$  between the polarization direction of polarizer and the rubbing direction of cell are shown in Figure 8c. It can be seen in this figure that no obvious scattering occurs in the field-off state in all angles. As the voltage is applied to the cell, the gel displays the anisotropic scattering state due to the formation of oriented LC multi-domains. The maximum scattering is obtained when the polarization direction of the polarizer is parallel to the rubbing direction of the cell, while the minimum scattering occurs when the polarizer is set to be perpendicular to the rubbing direction of the cell. Therefore, the gel can be used as a switchable scattering polarizer whose field-on and field-off states can be controlled by an ultra-low voltage of only about 3 V. Figure 8d shows the transmittance spectrum of 0.2 wt % F8BT LC gel in the wavelength range from 400 to 800 nm. The transmittances were recorded as the polarization direction of polarizer was parallel to the rubbing direction of cell at field-off (0 V) and field-on (3.6 V) states. Although the transmittance of the gel has a little loss for the absorption at the 450 nm at the field-off state, the gel presents a low transmission state for a broadband range (500 nm–800 nm) as the electric field turns on. The rise and decay times of the supramolecular gel with the F8BT concentrations of 0.2, 0.4, and 0.6 wt % were obtained for (3, 90), (6, 58), and (10, 52) ms under 5 V bias voltage, respectively. The switching times of the supramolecular gel are influenced by the amount of the gelator F8BT, and the increase in the concentration of the F8BT polymers leads to longer rise time and shorter decay time because of stronger attraction from the oriented fibrous structure. Although the response time is not fast enough now, we consider that the problem could be solved by doping some nanoparticles or modulating a suitable cell gap in the near future.<sup>47</sup>

Figure 9 shows the transmittance–voltage curves of the supramolecular LC gels with 0.2, 0.5, and 1.0 wt % of F8BT in a 9  $\mu$ m thick LC cell with unrubbed film. As the supramolecular LC gels formed in the cells with unrubbed polyimide film, we found that the gel exhibits an unstable light scattering phenomenon. The reason should be due to the formation of the random polymer network, as shown in Figure 4b, for the absence of the alignment interface. These fibrous fibers that induce the gel show the light scattering property in the field-off state for the formation of the LC multi-domains. However, with the lack of an alignment interface, the F8BT molecules were

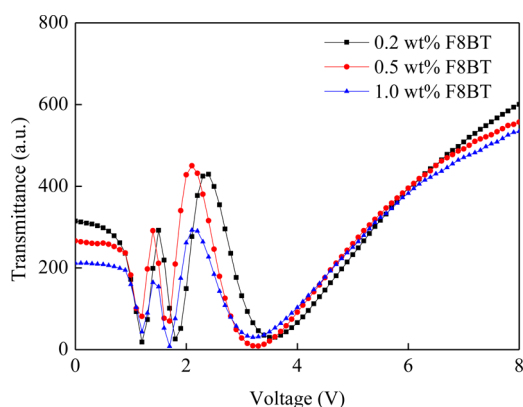


**Figure 9.** Transmittance–voltage curves of the supramolecular LC gels with 0.2, 0.5, and 1.0 wt % of F8BT in a 9  $\mu\text{m}$  thick LC cell with unrubbed film. Without the aid of an alignment interface, the supramolecular LC gel exhibits unstable electro-optical properties.

randomly dispersed, such that the strongly  $\pi$ – $\pi$  stacking structure could not be formed after the sol–gel transition. It is believed that the  $\pi$ – $\pi$  interactions between the F8BT molecules and LC molecules become too weak to avoid the LC molecules rotating as the electric field turns on. Therefore, this supramolecular LC gel with random fibers is very unstable and has difficulty operating its electro-optical properties. To sum up, effectively combining the supramolecular  $\pi$ -conjugated gelator and LC molecules in a cell with rubbed alignment interface succeeds in generating a new kind of anisotropic scattering LC physical gel with ultra-low operating voltage and extremely high contrast ratio, which provides great possibility for application in various electro-optical devices such as tunable polarizers, transfective displays, and polarized light modulators.

#### 4. CONCLUSION

In summary, we report a new type of supramolecular LC gels which are formed by the fibrous self-assembly of the polyfluorene-based polymer F8BT in nematic LC E7. This new material can form a functional physical network through the  $\pi$ – $\pi$  stacking interactions between the  $\pi$ -conjugated main chains of the F8BT molecules. As the molecular self-assembly occurs in the anti-parallel rubbed LC cell, the oriented fibrous aggregates induce the formation of the anisotropic fibers which are perpendicular to the director of the LC molecules. The rubbed interface between the LC molecules and polyimide layer greatly influence the characteristics of the LC physical gels. In the paper, we first report that the supramolecular LC physical gels with aligned  $\pi$ -conjugated fibrous structures exhibit significant anisotropic scattering. The incident light is highly scattering as the light polarization is parallel to the long-axis direction of LC molecules and the main-chain direction of the F8BT molecules. Opposite to the LC gels formed by low-molecular-weight gelators which need high voltage to drive LCs, the driving voltage required to switch the transparent and scattering states in the supramolecular LC gels is extremely low, only 2.7 V. In addition, the contrast ratio can be achieved as high as exceeding 1000. Although the response times of the supramolecular LC physical gels still need to improve, the excellent characteristics such as dramatically decreased driving voltage and high contrast ratio provide the possibility to be a promising candidate for use in transfective display technology and electrically switchable smart polarizer.

#### ■ ASSOCIATED CONTENT

##### Supporting Information

Results of representative DSC data (Figure S1), polarized PL spectra for samples prepared in cells without rubbing treatment (Figure S2), and the  $^1\text{H}$  NMR spectroscopy of F8BT polymers in  $\text{CDCl}_3$  with different temperatures (Figure S3). This material is available free of charge via the Internet at <http://pubs.acs.org>.

#### ■ AUTHOR INFORMATION

##### Corresponding Author

\*E-mail: [cychao@phys.ntu.edu.tw](mailto:cychao@phys.ntu.edu.tw) (C.-Y.C.).

##### Notes

The authors declare no competing financial interest.

#### ■ ACKNOWLEDGMENTS

One of us (C.-Y.C.) would like to thank National Taiwan University, National Science Council, and Ministry of Education of the Republic of China for financial supports in this work.

#### ■ REFERENCES

- (1) Abdallah, D. J.; Weiss, R. G. Organogels and Low Molecular Mass Organic Gelators. *Adv. Mater.* **2000**, *12*, 1237–1247.
- (2) Brotin, T.; Utermöhlen, R.; Fages, F.; Bouaslaurent, H.; Desvergne, J.-P. A Novel Small Molecular Luminescent Gelling Agent for Alcohols. *J. Chem. Soc., Chem. Commun.* **1991**, *6*, 416–418.
- (3) Geiger, C.; Stanescu, M.; Chen, L. H.; Whitten, D. G. Organogels Resulting from Competing Self-Assembly Units in the Gelator: Structure, Dynamics, and Photophysical Behavior of Gels Formed from Cholesterol-Stilbene and Cholesterol-Squaraine Gelators. *Langmuir* **1999**, *15*, 2241–2245.
- (4) George, M.; Weiss, R. G. Molecular Organogels. Soft Matter Composed of Low-Molecular-Mass Organic Gelators and Organic Liquids. *Acc. Chem. Res.* **2006**, *39*, 489–497.
- (5) Hanabusa, K.; Hiratsuka, K.; Kimura, M.; Shirai, H. Easy Preparation and Useful Character of Organogel Electrolytes Based on Low Molecular Weight Gelator. *Chem. Mater.* **1999**, *11*, 649–655.
- (6) Hanabusa, K.; Tanaka, R.; Suzuki, M.; Kimura, M.; Shirai, H. Excellent Gelators for Organic Fluids: Simple Bolaform Amides Derived from Amino Acids. *Adv. Mater.* **1997**, *9*, 1095–1097.
- (7) Kamikawa, Y.; Kato, T. Color-Tunable Fluorescent Organogels: Columnar Self-Assembly of Pyrene-Containing Oligo(glutamic acid)s. *Langmuir* **2007**, *23*, 274–278.
- (8) Terech, P.; Weiss, R. G. Low Molecular Mass Gelators of Organic Liquids and the Properties of Their Gels. *Chem. Rev.* **1997**, *97*, 3133–3159.
- (9) van Esch, J. H.; Feringa, B. L. New Functional Materials Based on Self-Assembling Organogels: From Serendipity towards Design. *Angew. Chem., Int. Ed.* **2000**, *39*, 2263–2266.
- (10) Guan, L.; Zhao, Y. Self-Assembly of a Liquid Crystalline Anisotropic Gel. *Chem. Mater.* **2000**, *12*, 3667–3673.
- (11) Guan, L.; Zhao, Y. Self-Assembled Gels of Liquid Crystals: Hydrogen-Bonded Aggregates Formed in Various Liquid Crystalline Textures. *J. Mater. Chem.* **2001**, *11*, 1339–1344.
- (12) Kato, T. Self-Assembly of Phase-Segregated Liquid Crystal Structures. *Science* **2002**, *295*, 2414–2418.
- (13) Kato, T.; Hirai, Y.; Nakaso, S.; Moriyama, M. Liquid-Crystalline Physical Gels. *Chem. Soc. Rev.* **2007**, *36*, 1857–1867.
- (14) Kato, T.; Kutsuna, T.; Hanabusa, K.; Ukon, M. Gelation of Room-Temperature Liquid Crystals by the Association of a trans-1,2-bis(amino)cyclohexane Derivative. *Adv. Mater.* **1998**, *10*, 606–608.
- (15) Kato, T.; Mizoshita, N.; Kishimoto, K. Functional Liquid-Crystalline Assemblies: Self-Organized Soft Materials. *Angew. Chem., Int. Ed.* **2006**, *45*, 38–68.

- (16) Sangeetha, N. M.; Maitra, U. Supramolecular Gels: Functions and Uses. *Chem. Soc. Rev.* **2005**, *34*, 821–836.
- (17) Hirai, Y.; Monobe, H.; Mizoshita, N.; Moriyama, M.; Hanabusa, K.; Shimizu, Y.; Kato, T. Enhanced Hole-Transporting Behavior of Discotic Liquid-Crystalline Physical Gels. *Adv. Funct. Mater.* **2008**, *18*, 1668–1675.
- (18) Mizoshita, N.; Monobe, H.; Inoue, M.; Ukon, M.; Watanabe, T.; Shimizu, Y.; Hanabusa, K.; Kato, T. The Positive Effect on Hole Transport Behaviour in Anisotropic Gels Consisting of Discotic Liquid Crystals and Hydrogen-Bonded Fibres. *Chem. Commun.* **2002**, *5*, 428–429.
- (19) Mizoshita, N.; Hanabusa, K.; Kato, T. Self-Aggregation of an Amino Acid Derivative as a Route to Liquid-Crystalline Physical Gels - Faster Response to Electric Fields. *Adv. Mater.* **1999**, *11*, 392–394.
- (20) Mizoshita, N.; Hanabusa, K.; Kato, T. Fast and High-Contrast Electro-Optical Switching of Liquid-Crystalline Physical Gels: Formation of Oriented Microphase-Separated Structures. *Adv. Funct. Mater.* **2003**, *13*, 313–317.
- (21) Nair, G. G.; Prasad, S. K.; Jayalakshmi, V.; Shanker, G.; Yelamaggad, C. V. Fast Responding Robust Nematic Liquid Crystalline Gels Formed by a Monodisperse Dipeptide: Electro-Optic and Rheological Studies. *J. Phys. Chem. B* **2009**, *113*, 6647–6651.
- (22) Tolksdorf, C.; Zentel, R. Reversible Physical Network Stabilized Ferroelectric Liquid Crystals. *Adv. Mater.* **2001**, *13*, 1307–1310.
- (23) Cardinaels, T.; Hirai, Y.; Hanabusa, K.; Binnemans, K.; Kato, T. Europium(III)-Doped Liquid-Crystalline Physical Gels. *J. Mater. Chem.* **2010**, *20*, 8571–8574.
- (24) Janssen, R. H. C.; Stumpf, V.; Broer, D. J.; Bastiaansen, C. W. M.; Tervoort, T. A.; Smith, P. Electrically Controlled Light Scattering from Thermoreversible Liquid-Crystal Gels. *J. Appl. Phys.* **2000**, *88*, 161–167.
- (25) Mizoshita, N.; Suzuki, Y.; Kishimoto, K.; Hanabusa, K.; Kato, T. Electrooptical Properties of Liquid-Crystalline Physical Gels: A New Oligo(amino acid) Gelator for Light Scattering Display Materials. *J. Mater. Chem.* **2002**, *12*, 2197–2201.
- (26) Suzuki, Y.; Mizoshita, N.; Hanabusa, K.; Kato, T. Homeotropically Oriented Nematic Physical Gels for Electrooptical Materials. *J. Mater. Chem.* **2003**, *13*, 2870–2874.
- (27) Tong, X.; Zhao, Y. Self-Assembled Cholesteric Liquid Crystal Gels: Preparation and Scattering-Based Electrooptical Switching. *J. Mater. Chem.* **2003**, *13*, 1491–1495.
- (28) Tong, X.; Zhao, Y.; An, B.-K.; Park, S. Y. Fluorescent Liquid-Crystal Gels with Electrically Switchable Photoluminescence. *Adv. Funct. Mater.* **2006**, *16*, 1799–1804.
- (29) Donley, C. L.; Zaumseil, J.; Andreasen, J. W.; Nielsen, M. M.; Sirringhaus, H.; Friend, R. H.; Kim, J.-S. Effects of Packing Structure on the Optoelectronic and Charge Transport Properties in Poly(9,9-di-n-octylfluorene-alt-benzothiadiazole). *J. Am. Chem. Soc.* **2005**, *127*, 12890–12899.
- (30) Keivanidis, P. E.; Howard, I. A.; Friend, R. H. Intermolecular Interactions of Perylene diimides in Photovoltaic Blends of Fluorene Copolymers: Disorder Effects on Photophysical Properties, Film Morphology and Device Efficiency. *Adv. Funct. Mater.* **2008**, *18*, 3189–3202.
- (31) Zheng, Z. J.; Yim, K.-H.; Saifullah, M. S. M.; Welland, M. E.; Friend, R. H.; Kim, J.-S.; Huck, W. T. S. Uniaxial Alignment of Liquid-Crystalline Conjugated Polymers by Nanoconfinement. *Nano Lett.* **2007**, *7*, 987–992.
- (32) Abbel, R.; Grenier, C.; Pouderoijen, M. J.; Stouwdam, J. W.; Leclère, P. E. L. G.; Sijbesma, R. P.; Meijer, E. W.; Schenning, A. P. H. J. White-Light Emitting Hydrogen-Bonded Supramolecular Copolymers Based on  $\pi$ -Conjugated Oligomers. *J. Am. Chem. Soc.* **2009**, *131*, 833–843.
- (33) Neher, D. Polyfluorene Homopolymers: Conjugated Liquid-Crystalline Polymers for Bright Blue Emission and Polarized Electroluminescence. *Macromol. Rapid Commun.* **2001**, *22*, 1366–1385.
- (34) O'Neill, M.; Kelly, S. M. Ordered Materials for Organic Electronics and Photonics. *Adv. Mater.* **2011**, *23*, 566–584.
- (35) Pei, Q.; Yang, Y. Efficient Photoluminescence and Electroluminescence from a Soluble Polyfluorene. *J. Am. Chem. Soc.* **1996**, *118*, 7416–7417.
- (36) Scherf, U.; List, E. J. W. Semiconducting Polyfluorenes - Towards Reliable Structure-Property Relationships. *Adv. Mater.* **2002**, *14*, 477–487.
- (37) Chen, J.-H.; Chang, C.-S.; Chang, Y.-X.; Chen, C.-Y.; Chen, H.-L.; Chen, S.-A. Gelation and Its Effect on the Photophysical Behavior of Poly(9,9-dioctylfluorene-2,7-diyl) in Toluene. *Macromolecules* **2009**, *42*, 1306–1314.
- (38) Lin, Z.-Q.; Shi, N.-E.; Li, Y.-B.; Qiu, D.; Zhang, L.; Lin, J.-Y.; Zhao, J.-F.; Wang, C.; Xie, L.-H.; Huang, W. Preparation and Characterization of Polyfluorene-Based Supramolecular  $\pi$ -Conjugated Polymer Gels. *J. Phys. Chem. C* **2011**, *115*, 4418–4424.
- (39) Rahman, M. H.; Liao, S.-C.; Chen, H.-L.; Chen, J.-H.; Ivanov, V. A.; Chu, P. P. J.; Chen, S.-A. Aggregation of Conjugated Polymers in Aromatic Solvent. *Langmuir* **2009**, *25*, 1667–1674.
- (40) Grell, M.; Redecker, M.; Whitehead, K. S.; Bradley, D. D. C.; Inbasekaran, M.; Woo, E. P.; Wu, W. Monodomain Alignment of Thermotropic Fluorene Copolymers. *Liq. Cryst.* **1999**, *26*, 1403–1407.
- (41) Hirai, Y.; Babu, S. S.; Praveen, V. K.; Yasuda, T.; Ajayaghosh, A.; Kato, T. Anisotropic Self-Assembly of Photoluminescent Oligo(p-Phenylenevinylene) Derivatives in Liquid Crystals: An Effective Strategy for the Macroscopic Alignment of  $\pi$ -Gels. *Adv. Mater.* **2009**, *21*, 4029–4033.
- (42) Kato, T.; Kutsuna, T.; Yabuuchi, K.; Mizoshita, N. Anisotropic Self-Aggregation of an Anthracene Derivative: Formation of Liquid-Crystalline Physical Gels in Oriented States. *Langmuir* **2002**, *18*, 7086–7088.
- (43) Lin, J.; Yu, Z.; Zhu, W.; Xing, G.; Lin, Z.; Yang, S.; Xie, L.; Niu, C.; Huang, W. A  $\pi$ -Conjugated Polymer Gelator from Polyfluorene-Based Poly(tertiary alcohol) via the Hydrogen-Bonded Supramolecular Functionalization. *Polym. Chem.* **2013**, *4*, 477–483.
- (44) Chen, Y.; Qian, J.; Liu, X. Y.; Zhuang, Q. X.; Han, Z. W. Synthesis and Photoluminescence Properties of Polybenzoxazoles Containing Perylenebisimide Functionalized Graphene Nanosheets via Stacking Interactions. *New J. Chem.* **2013**, *37*, 2500–2508.
- (45) Guo, J.; Xu, Y. H.; Jin, S. B.; Chen, L.; Kaji, T.; Honsho, Y.; Addicoat, M. A.; Kim, J.; Saeki, A.; Ihee, H.; Seki, S.; Irie, S.; Hiramoto, M.; Gao, J.; Jiang, D. L. Conjugated Organic Framework with Three-Dimensionally Ordered Stable Structure and Delocalized  $\pi$  clouds. *Nat. Commun.* **2013**, *4*, 2736.
- (46) Mizoshita, N.; Kutsuna, T.; Hanabusa, K.; Kato, T. Smectic Liquid-Crystalline Physical Gels. Anisotropic Self-Aggregation of Hydrogen-Bonded Molecules in Layered Structures. *Chem. Commun.* **1999**, *9*, 781–782.
- (47) Tripathi, P. K.; Misra, A. K.; Manohar, S.; Gupta, S. K.; Manohar, R. Improved Dielectric and Electro-Optical Parameters of ZnO Nano-Particle (8% Cu<sup>2+</sup>) Doped Nematic Liquid Crystal. *J. Mol. Struct.* **2013**, *1035*, 371–377.